J Mater Sci: Mater Med (2007) 18:787–796
DOI 10.1007/s10856-006-0010-4

Structural and spatially resolved studies on the hardening of a commercial resin-modified glass-ionomer cement

Ricardo A. Pires · Christian Fernandez · Teresa G. Nunes

Received: 12 September 2005 / Accepted: 8 December 2005 / Published online: 2 December 2006

Abstract A commercial photopolymerizable resin-modified glass-ionomer (Fuji II LC) was studied using a variety of nuclear magnetic resonance (NMR) techniques. ^{1}H and ^{19}F stray-field imaging (STRAFI) enabled to follow the acid–base reaction kinetics in self-cured (SC) samples. Gelation and maturation processes with 25 min and 40 h average time constants, respectively, were distinguished. In self- & photo-cured (SPC) samples, two processes were also observed, which occurred with 2 s and 47 s average time constants. ^{1}H, ^{27}Al and ^{29}Si magic angle spinning (MAS) NMR, ^{13}C cross-polarization (CP)/MAS NMR and ^{27}Al multiple quanta (MQ)MAS NMR spectroscopy were used to obtain structural information on the glass and cements that were either SC or SPC. The presence of methacrylate groups was identified in the solid component. Unreacted hydroxyl ethylmethacrylate (HEMA) was detected in self-cured cement. ^{27}Al data showed that approximately 28% and 20% of Al is leached out from glass particles in SC and SPC samples, respectively. The upfield shift detected in ^{29}Si MAS NMR spectra of the cements is consistent with a decrease in the number of Al species in the second coordination sphere of the silicon structures. Scanning electron microscopy (SEM) showed existence of 3D shrinkage of the cement matrix in photo-cured cements.

R. A. Pires · T. G. Nunes (✉)
Departamento de Engenharia de Materiais, Instituto Superior Técnico, Universidade Técnica de Lisboa, Av. Rovisco Pais, 1, 1049-001 Lisboa, Portugal
e-mail: Teresa.Nunes@ist.utl.pt

Present Address:
R. A. Pires
3B's Research Group, Department of Polymer Engineering, University of Minho, Campus de Azurém, 4800-058 Guimaraes, Portugal

C. Fernandez
Laboratoire Catalyse et Spectrochimie, CNRS/ENSICAEN, 6 bd du Maréchal Juin, 14050 Caen Cedex, France

1 Introduction

Glass-ionomer cements (GICs) were first reported for use in restorative dental treatment in the 1970s [1–3]. Since then, a series of different studies have been published concerning its structure [4–6] or setting chemistry [4, 7–11] and the work carried out over the past years have been also reviewed [12, 13]. When GIC are applied in oral environment, the major problem is the setting reaction being readily affected by the presence of moisture, like saliva; then, at the early stage of setting, its hardened mass becomes brittle on its surface ending up with deteriorations of the physical properties. Aiming at improving the mechanical properties and lowering the solubility of GICs, resin-modified glass-ionomer cements (RMGIC) were developed [14]. These are hybrid materials with dual-cure properties that contain in the formulation some polymerizable functional methacrylate groups and a photoinitiator, and undergo both an acid–base reaction (like a conventional GIC) as well as curing by photoinitiation of methacrylate carbon double bonds. Thus, setting occurs initially through the neutralizing reaction of the glass powder with the acidic polymer groups concurring with the polymerizing reaction of

hydrophilic monomers present therewith, whereby the initial setting reaction can proceed rapidly sufficient to obtain a GIC much less sensitive to water at the initial stage of setting. Hence, in RMGICs, water is in part replaced by a photopolymerizable monomer (like HEMA) and glass particles are eventually treated with a vinylic silane, which acts as a coupling agent. The formulation may have also incorporated a chemical curing tertiary amine–peroxide reaction to polymerize the methacrylate double bonds and these materials are then known as tri-cure RMGICs. RMGICs have been shown to adhere to enamel and dentine [15] and, like conventional GICs, these materials enable a continual fluoride release, thus reducing incidence of secondary caries. The long-term post-irradiation hardness of Fuji II LC and other RMGICs were evaluated and compared with conventional GICs, while storing the cements in saline at 37°C [16]. The obtained results showed that RMGICs are formulated so that their properties are equivalent to conventional GICs and also agreed well with previously reported findings on the retardation of the setting reaction of a GIC prepared with 50/50 water/HEMA, which was due to the presence of HEMA replacing water and resulted in a weaker cement [17].

Recently, new results were reported on GIC formation and structural characterization, using Stray-Field MRI (STRAFI) and multinuclear magnetic resonance [10]. The STRAFI-MRI technique showed the existence of two processes during the GIC curing reactions. A faster one with a time constant of the order of minutes, assigned to the gelation phase (leaching of cations from the glass to the matrix) and a slower one with a time constant in the range of 1 day, assigned to the maturation phase (cross-linking of the polymer chains by the leached cations) [10]. Using 2D ^{27}Al triple-quantum MAS technique (MQMAS), it was shown that in the gelation phase are leached out from the glass Al^{3+}, which was initially present in a 4-, 5- and 6-coordinate environment, and Sr^{2+}. Moreover, in the cement, two 4-coordinated and two 6-coordinated environments were detected without any detectable 5-coordinated aluminium, result that is consistent with a heterogeneous distribution of the 5-coordinated aluminium, predominant at the glass particles surface. ^{29}Si MAS NMR spectra showed the existence of re-condensation of the silicon tetrahedra upon the acid attack [10].

A methodology similar to the one used to study the Fuji II system [10] was applied to another commercial GIC, Fuji II LC (F2LC), which is a RMGIC. Accordingly, structural information was obtained from the glass, before the curing reactions, and from the cements using liquid state ^{1}H NMR, solid state ^{1}H, ^{13}C CP, ^{27}Al (1D and 2D MQ) and ^{29}Si MAS NMR spectroscopy. Additionally, the kinetics of the acid–base reaction (self-cured samples) and the acid–base and photopolymerization reactions (self- & photo-cured samples) were monitored using STRAFI-MRI and the extension of the curing reaction were obtained. To our knowledge, no NMR evidence was yet reported on the presence of an acid–base reaction in photo-cured RMGICs. SEM was also used to characterize the cement structure.

2 Materials and methods

A resin-modified glass-ionomer, Fuji II LC (F2LC), was supplied by GC Corporation. The solid (shade A2, batch 0209111) and the liquid (batch 020661) components were mixed to obtain the cement paste. According to the manufacturers, the formulation may include a fluoroaluminosilicate glass treated with a vinylic silane coupling agent, a polyacid such as polyacrylic acid, a polyketone as camphorquinone, a reducing agent (usually an amine), eventually an inorganic filler (also silanated and that does not react with the acid) and benzoyl peroxide to chemically initiate the polymerization of the monomer present in the liquid component; this component contains water, in which is emulsified an hydrophilic monomer such as HEMA.

Two sets of cements were prepared: (a) Self-cured and (b) Self- & photo-cured, which was obtained following the instructions from the manufacturers. A conventional quartz-tungsten-halogen light curing unit (Optilux Demetron Research Corp., Danbury, CT, USA 401), was used to irradiate the pastes (470 nm, 500 mW/cm^2) over cumulative periods until a total of 90 s was reached.

One-dimensional ^{1}H STRAFI images, projections along an axis, were acquired from the pastes, 6 min after mixing the solid and the liquid components, and from the cured cements, either self- or self- & photo-cured, on a Bruker MSL 300 P spectrometer with a superconducting solenoid coil which generates a 37.5 T/m static magnetic field gradient near the edges of the coil. A dedicated STRAFI probe was used which was tuned to 123.4 MHz, the resonance frequency of ^{1}H and ^{19}F at 2.9 T and 3.1 T, respectively; accordingly, were sequentially observed ^{1}H and ^{19}F projections about 4.9 mm separated. The magnetization was recorded as multiple 8 spin-echo trains. Each echo train was generated by the radio frequency (RF) pulse sequence $90°_x$–τ–$[90°_y$–τ–echo–$\tau]_8$, where $90°_{x,y}$ represents a 90° pulse of relative phase x or y and τ is a short

time delay; the RF pulse duration (t_p) and echo time (TE) were 10 μs and 35 μs, respectively (see [18] for details). Each data slice in the STRAFI-MRI profiles (Fig. 2a, b) is the result of the summation of the 8 echoes, recorded over 280 μs. The samples were contained in cylindrical glass vials with 7 mm diameter and 4 mm height (internal dimensions). A plastic disc was glued to the outside bottom of the glass vial to be used as reference for the magnetization intensities. Additionally, a cylindrical glass spacer about 5 mm height was introduced between the cements and the plastic disc in order to avoid the overlap of ^{1}H and ^{19}F 1D profiles. In STRAFI, the linear resolution Δx can be estimated by $\sqrt{3} \cdot \pi/(t_p \cdot \gamma_H \cdot G_z)$, with t_p the RF pulse duration that is related to the frequency range to be excited, γ_H the proton gyromagnetic ratio (267.5 Mrad/T) and G_z the magnetic field gradient along the Z axis, also the axis of the static magnetic field [19] providing a figure of less than 100 μm for the excited slice thickness.

A ^{1}H spectrum from the liquid component, in $CDCl_3$ with TMS for the reference signal at 0 ppm, was acquired also on a Bruker MSL 300 P spectrometer operating at 300.13 MHz, using a single RF pulse with 5 μs duration (corresponding to 90° magnetization tip angle, β) and 20 s recycling delay.

^{1}H MAS NMR and ^{13}C CP/MAS NMR spectra of the solid component, SC and SPC cements were acquired on the same spectrometer. The ^{1}H spectra were recorded at 10 kHz spinning speed on 4 mm o.d. zirconia rotors, with a pulse duration of 2 μs ($\beta \approx 90°$). The ^{13}C spectra were obtained at 4 kHz spinning speed on 7 mm o.d. zirconia rotors, with a pulse duration of 5 μs ($\beta = 90°$), 4 ms contact time and 20 s recycling delay. ^{27}Al and ^{29}Si MAS NMR spectra of the solid component, SC and SPC cements were observed at 78.17 MHz and 59.60 MHz, respectively, using a single RF pulse sequence. ^{27}Al spectra were acquired on 4 mm o.d. zirconia rotors, with a pulse duration of 0.6 μs ($\beta \approx 15°$), a recycling delay of 3 s and a spinning speed of 10.0 kHz. ^{29}Si MAS spectra were acquired using 7 mm o.d. zirconia rotors, with 3 μs pulse duration ($\beta = 45°$), 90 s recycling delay and 4.5 kHz spinning rate. ^{27}Al MQMAS NMR spectra of SC and SPC cements were acquired on a Bruker AVANCE 400 operating at 104.33 MHz, on 4 mm o.d. zirconia rotors, using a Multiplex (SPAM) acquisition sequence [20], pulse lengths of 2.5, 0.9 and 7.5 μs, a recycling delay of 1 s and 14.0 kHz spinning rate.

SEM micrographs of the glass, SC and SPC cements were acquired on a Hitachi S-2400, using a tungsten filament. Energy dispersive spectroscopy (EDX) was also run in the same microscope using energy of 25 keV, to obtain the qualitative composition of the F2LC glass component.

3 Results and discussion

3.1 Characterization of the liquid and solid component

Figure 1 shows the ^{1}H NMR spectrum of the liquid component in $CDCl_3$. Major ^{1}H signals are assigned to HEMA: at $\delta(CH_3)$ = 1.95 ppm, $\delta(CH_2$-pendant) = 3.86 and 4.27 ppm, $\delta(CH_2$-methacrylate) = 5.60 and 6.16 ppm and δ(OH) = 5.75 ppm. Additionally, ^{1}H NMR shows the presence of free water resonance at about 4.7 ppm and less intense signals, which are possibly from additional methacrylate monomers at low concentration, like triethylene glycol dimethacrylate. The ^{1}H MAS NMR spectrum of the solid component is shown in Fig. 4a. Strong line broadening does not allow performing a full spectrum assignment. However, signals from methacrylate groups are identified at $\delta(CH_2$-methacrylate) $\approx$ 5.4 ppm and 6.1 ppm and at $\delta(CH_3$-methacrylate) $\approx$ 1.8 ppm.

The SEM-EDX spectrum showed that aluminium, silicon and strontium are present in the solid component. The ^{27}Al and ^{29}Si MAS NMR spectra of the solid component are similar to the previously reported spectra on the solid component of the conventional GIC FUJI II [10] and show the presence of three aluminium species, 4-, 5- and 6-coordinated, and one highly distributed silicon species at an average resonance frequency of Q^4 tetrahedra with 1–2 aluminium atoms in the second coordination sphere. In the case of

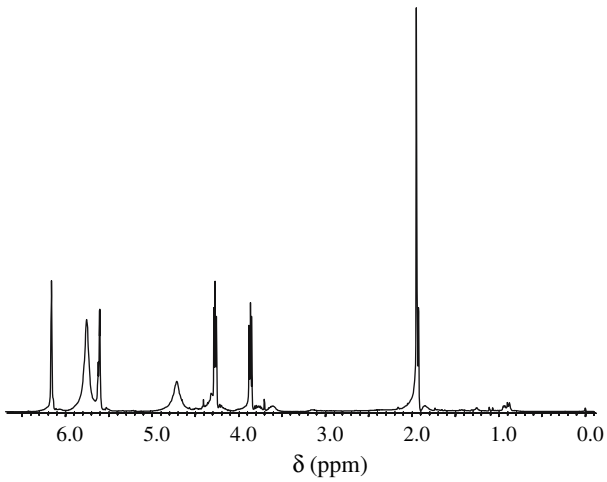

Fig. 1 ^{1}H NMR spectrum of the liquid component of F2LC, in $CDCl_3$

the silicon tetrahedra the position of the signal is also consistent with Q^3 tetrahedron, that is, with no Al in the second coordination sphere [21].

3.2 Kinetic study

The spatially resolved kinetics for the acid–base and photo-curing reactions of F2LC was followed by ^1H STRAFI-MRI. This technique was introduced by Samoilenko et al. [22] and allows to image liquids, gels and rigid solids. Thus, it enables following phase transitions that occur during the hardening of materials like Portland [23] and glass-ionomer cements [10, 24] and photopolymerizable dental resins [18, 25–27]. The signal intensity is related to the ^1H concentration but the magnetization decay is strongly weighted particularly by spin–spin and spin–lattice in the rotating frame relaxations processes, which have T_2 and $T_{1\rho}$ relaxation times, respectively. These two parameters are shorter for rigid solids and longer for liquids. Consequently, higher intensity signals are observed in liquids as compared with solids when similar spin-echo acquisitions are performed [23]. Hence, by monitoring the variation of magnetization intensity with time, it is then possible to follow the liquid–gel–solid phase transitions that may occur during curing reactions.

For the follow-up of the RMGIC self-curing reactions, magnetization profiles were acquired 6 min after the paste preparation and then periodically, as follows: (a) every 5 min during the first half hour, (b) every 10 min up to 4 h 30 min and (c) every hour until a total of 72 h was reached. Typical 1D projections of SC cement, recorded 6 min and 72 h after start mixing the solid and the liquid components, are shown in Fig. 2a, which represents the evolution of ^1H magnetization profiles with accumulated setting time; it must be noticed that, in these figures, the profiles are rotated of 90° and, consequently, the sample surfaces and the reference signals obtained from plastic discs, are shown on the left- and on the right-side of the plots, respectively. For the follow-up of the self- & photo-curing reactions, magnetization profiles were acquired 6 min after the paste preparation and after cumulative irradiating periods until a total of 90 s was reached. Typical 1D profiles of SPC cement obtained 6 min after start mixing the liquid and solid components and after 90-s irradiation period are presented in Fig. 2b. Images on Fig. 2 also comprise ^{19}F profiles, which are shown about 4.9 mm shifted from the ^1H profile (displayed at 0–4.2 mm depth) and, consequently, appears at 4.9–9 mm.

The first general observations are the decrease in signal intensity and the narrowing of the profiles during

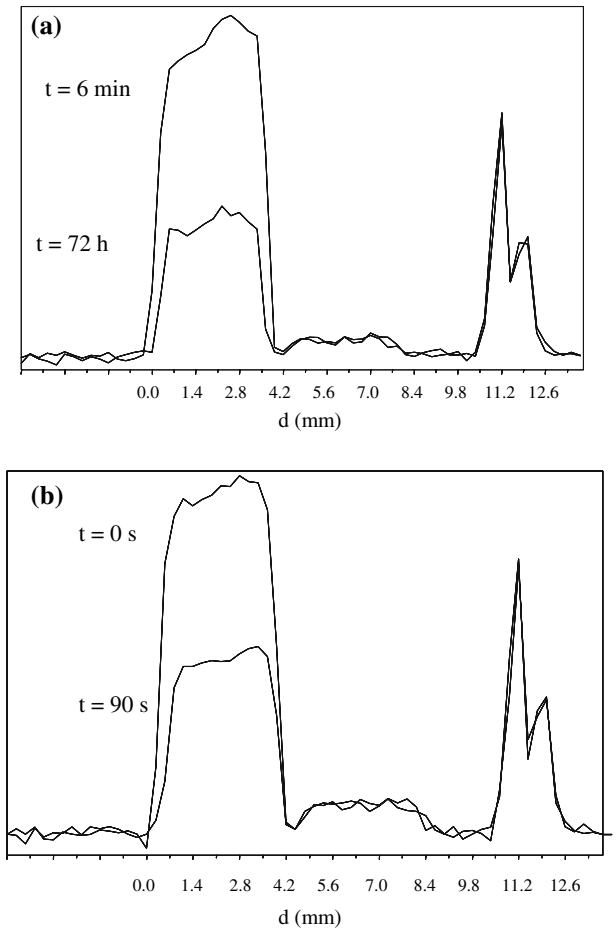

Fig. 2 ^1H STRAFI MRI profiles of SC (**a**) and SPC (**b**) F2LC cements. ^1H magnetization profiles for various irradiation times. The sharp signal shown on the right side of the profiles is from a commercial plastic disc placed outside the paste container, which were used as a reference for the magnetization intensities; the ^1H signal from the glue used to support the apparatus is also observed at $d \approx 12.0$ mm

the curing reactions. The latter effect is particularly associated with contractions during polymerization and hence overall volume reduction. Because extensive water evaporation is not expected during the curing process, the decrease of magnetization intensity with exposure time is clearly associated to the loss of proton mobility with evolving reactions. This fact enables mapping an estimate of the extent of the reaction.

In SC cement (Fig. 2a), major differences in ^1H magnetization intensities are observed between the first and the last acquired profiles, which are not noticed for ^{19}F profiles that seem unchangeable within the limitation of the obtained signal to noise ratios; this observation is consistent with non-involvement of fluorine atoms in cement setting during the observation period (72 h). Figure 3a represents the ^1H magnetization map for slices at different depths of the hardening

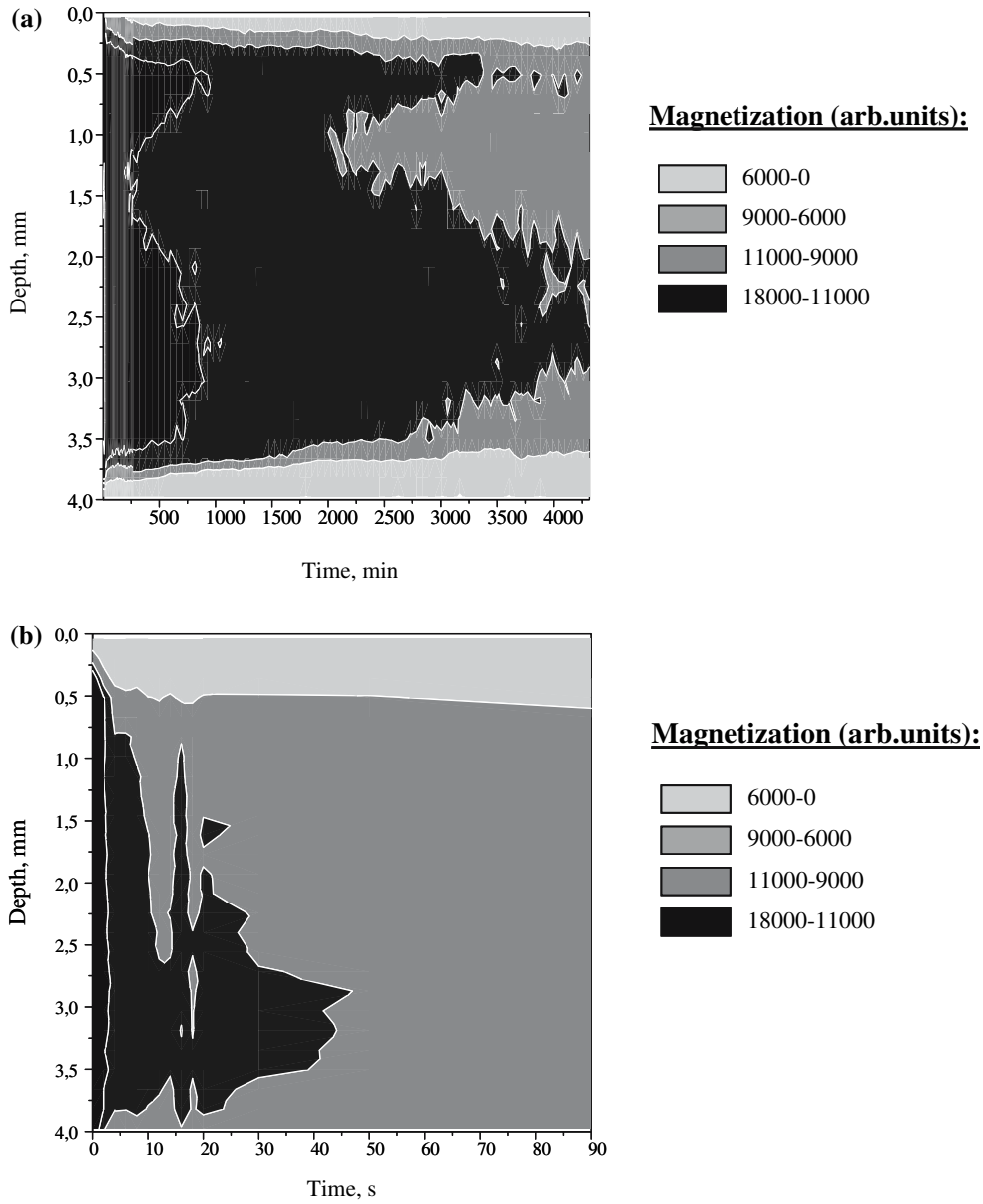

Fig. 3 Map of the magnetization distribution with the depth of the sample and the (**a**) irradiation time of SPC cement and (**b**) curing time of SC cement

cement obtained over 72 h, where a different colour is assigned to each of four different magnetization ranges (the linear resolution was less than 100 μm as already mentioned in Sect. 2); the grey scale represents also a mobility grade with more mobile domains being shown with darker colours. Fittings of the magnetization intensities recorded from three different slices as a function of time were performed using double exponential functions and the corresponding two time-constants, with average values of 25 min and 40 h, are shown in Table 1. These data are in agreement with the presence of gelation (faster process with the shorter time-constant) and maturation processes, as previously reported on conventional GICs [10]. Additionally, it is clear that, while gelation occurs with similar spatially resolved rates, the maturation process seems to be faster near the surface than in the cement bulk. Although we are unable to fully explain the variation of the kinetics with sample depth, it should be pointed out here that sedimentation of the glass particles is expected to contribute for the anisotropy of the hardening reaction. A similar observation was already reported on the setting of Portland Type I cement [28]. Moreover, while gelation rates are comparable to previously reported data on the conventional GIC Fuji II (29 min, average value), maturation occurs much more slowly (25 h in Fuji II). In fact, the acid–base reaction is expected to be retarded in RMGICs, as compared with conventional GICs, due to the following reasons: (a) water is partially replaced by HEMA

Table 1 Time constants of the double exponential functions that best fit the slice intensity decay at the indicated depth of the ^{1}H STRAFI-MRI profiles obtained from F2LC self-cured over 72 h

Depth (mm)	t_1 (min)	t_2 (h)
0.8	27.8 ± 2.2	28.8 ± 3.6
2.0	24.3 ± 1.7	45.0 ± 7.1
2.8	23.0 ± 1.8	45.9 ± 7.0

(with lower dielectric constant); (b) in this medium, the polyacid coils up more tightly and (c) glass particles are surface coated with a vinylic silane. For the study of SPC cements, 1D profiles were acquired as a function of irradiation time (t), starting 6 min after the paste preparation (t = 0 s) and ending following 90 s cumulative irradiation time (t = 90 s). Magnetization evolution as a function of irradiation time is presented in Fig. 3b and the first and the last acquired profiles are shown in Fig. 2b. Double-exponential functions were used to fit magnetization decays obtained from slices at three different depths, 2.1, 2.6 and 3.3 mm. Thus, two time-constants were obtained, which are shown in Table 2, that appear to correspond to two processes, with different time scales; a faster one with an average time constant of about 2 s and a slower one with an average time constant of about 47 s. At present, it is difficult to explain this result; a faster mechanism is usually related to a chemically controlled process while diffusion-controlled processes occur at reduced rates in a cross-linked network [29]. For the faster mechanism, the observed time constant changes with depth are within the errors associated with the determinations; however, for the slower process, the errors are of the order of the time constants, not enabling any conclusion to be taken. Due to the presence of glass particles, light scattering must also influence the rate of the photo-curing reactions [30].

Sigmoidal functions were previously used to fit STRAFI photopolymerization data on dental resins, generating time constants of 3.3 s [31] and 8.1 s [18]. These results are comparable to the time constant obtained for the first process (chemically controlled) but, because the fitting functions used in the present work were double exponentials, no further comments are allowed at this stage.

Table 2 Time constants of the double exponential functions that best fit the slice intensity decay at the indicated depth of the ^{1}H STRAFI-MRI profiles obtained from F2LC self- & photo-cured over 90 s (470 nm, 500 mW/cm^2)

Depth (mm)	t_1 (s)	t_2 (s)
2.1	1.6 ± 0.5	>32
2.6	1.8 ± 0.4	>66
3.3	1.4 ± 0.4	>43

3.3 Characterization of the curing reactions

Solid state NMR, which is a very informative technique for materials characterization, was used to probe the environment of ^{1}H, ^{13}C, ^{27}Al and ^{29}Si nuclei in the cements, after the curing reactions (SC and SPC cements). The corresponding ^{1}H MAS NMR spectra are shown in Fig. 4b and c. Beyond the signals from methacrylate groups, already mentioned in Sect. 3.1, the ^{1}H MAS NMR spectrum of SC cement displays two additional signals at $\delta \approx 0.9$ and 4.3 ppm, which are assigned to CH_3 and CH_2 groups, respectively, that should be from HEMA, also detected in the liquid component. Only one broad ^{1}H signal was observed from SPC cement (with about 7 ppm full width at half maximum, FWHM); the broadening effect is due to strong homonuclear dipolar coupling interactions, which are higher than the selected MAS rate. This result indicate that, in this cement, protons are less mobile and most probably at shorter distances, as expected when occur both photopolymerization and cross-linking of polymer chains promoted by cations leached from glass particles.

Similar ^{13}C CP/MAS spectra were recorded from SC and SPC cements (Fig. 5), which display signals from the methacrylate polymeric fraction observed at $\delta(CH_3$-methacrylate) ≈ 22.8–16.1 ppm, $\delta(CH_2$ and CH polymeric) ≈ 45.1–30.7 ppm, $\delta(CH_2$-pendant) ≈ 72.5–54.5

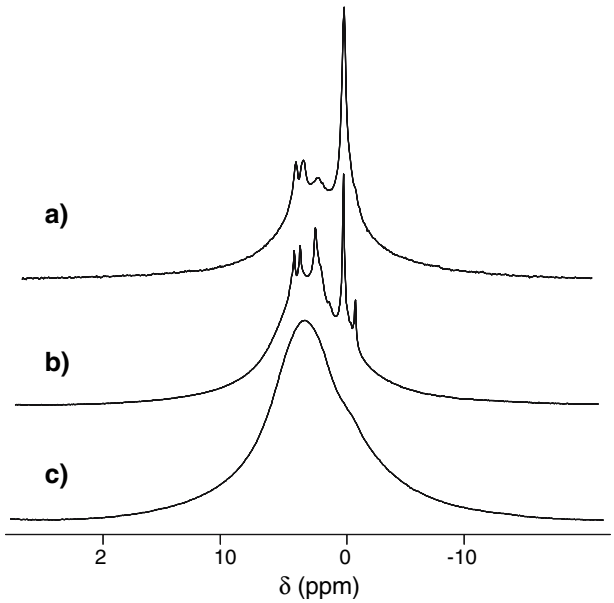

Fig. 4 ^{1}H MAS NMR spectra of the glass (**a**), self-cured (**b**) and self- & photo-cured (**c**) F2LC cement

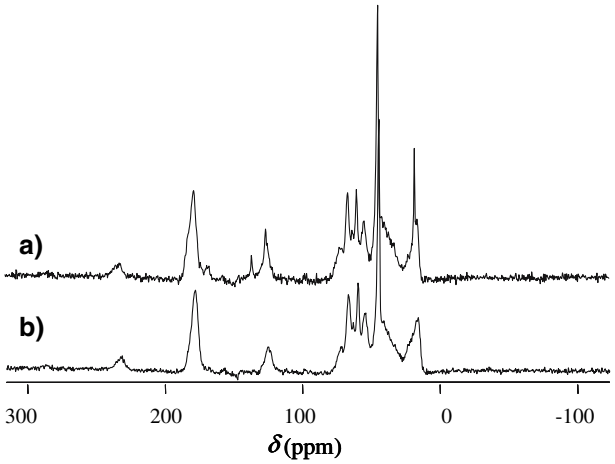

Fig. 5 ^{13}C CP/MAS NMR spectra of the self-cured (**a**) and self- & photo-cured (**b**) F2LC cement

ppm and $\delta(CO) \approx 178.8$ ppm. SC cement spectrum presents additional signals at $\delta(CH_3$-methacrylate$) \approx 18.1$ ppm, $\delta(CH_2$-methacrylate$) \approx 126.1$ ppm, $\delta(C) \approx 136.4$ ppm and $\delta(CO) \approx 168.9$ ppm, which are assigned to unreacted HEMA; HEMA signals from CH_2 groups are at $\delta(CH_2$-pendant$) \approx 66.7$ and 60.1 ppm but not well resolved due to overlapping with resonances from other unidentified polymeric methacrylates.

The aluminium environments were probed by ^{27}Al MAS NMR spectra acquired at 78.17 MHz from the solid component, SC and SPC cements. All the signals are broadened (Fig. 6) due to the interaction of the electric quadrupole moment (eQ) of ^{27}Al (spin 5/2) with the electric field gradient at the nucleus (eq), which is present due to the asymmetry of local electron distribution. This quadrupolar interaction is described by the quadrupolar coupling constant ($C_q = e^2qQ/h$) and the asymmetry parameter, η. The stronger the quadrupolar interaction, the broader the NMR signal, being more difficult to distinguish between different species. Hence, to obtain additional information on the aluminium surroundings were acquired ^{27}Al MQMAS NMR spectra of SC and SPC cements at 104.31 MHz (Fig. 7). While with MAS technique the dipolar and first order quadrupolar broadening can be reduced and in some cases zeroed, the second order quadrupolar broadening is maintained. All these interactions can be reduced with the MQMAS technique [32–35] enabling each aluminium environment to be distinguished. Therefore, the second order quadrupolar interaction is present in the projections represented horizontally but is zeroed in the vertical projections (Fig. 7). Hence, these spectra allowed estimating the isotropic chemical shift (δ_{iso}) and C_q, which can be used to obtain the aluminium coordination and to probe the asymmetry of local electron distribution. In

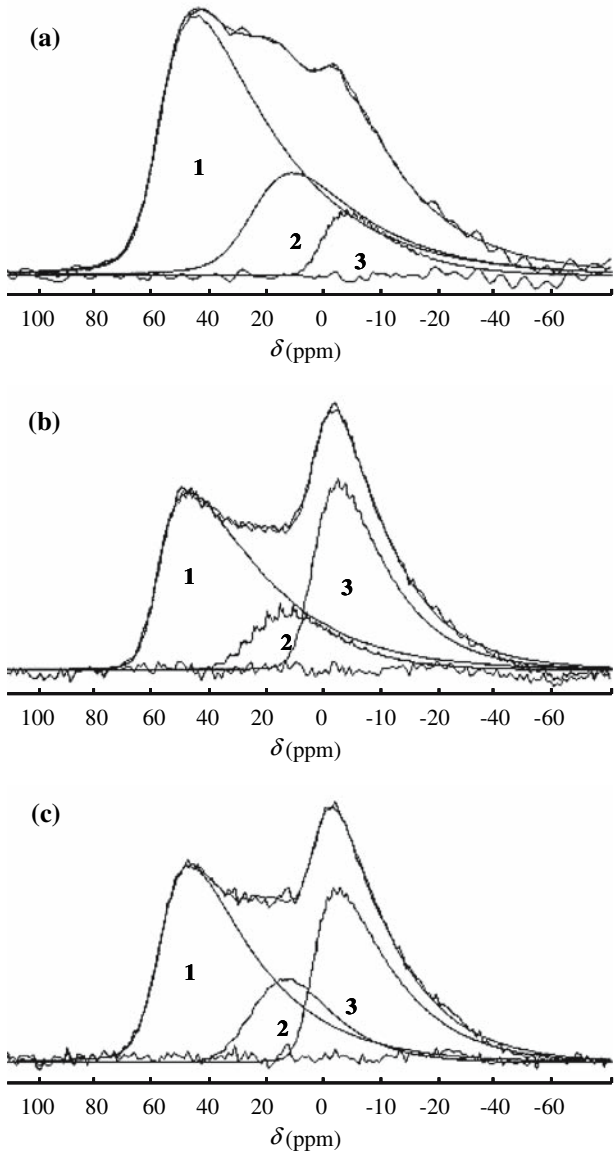

Fig. 6 ^{27}Al MAS spectra recorded at 78.17 MHz from the glass (**a**) and from F2LC cements either self-cured (**b**) or self- & photo-cured (**c**)

general, 4-, 5- and 6-coordinated species have δ_{iso} and C_q within: 88–55 ppm, 30–40 ppm, 1–15 ppm and 1–10 MHz, 3–10 MHz, 1–10 MHz, respectively [32].

Data obtained from ^{27}Al MQMAS experiments were used as input parameters for the fittings of 1D ^{27}Al MAS NMR spectra, which were performed using the software program *dmfit* [36] (Table 3). From this analysis, the solid component presents three main aluminium environments with 4, 5 and 6 coordinations and 65, 27 and 8%, relative concentrations, respectively. The acid–base reactions of SC cement reduced the concentration of the 4-coordinated species by 15% and the 5-coordinated species by 13%, increasing the

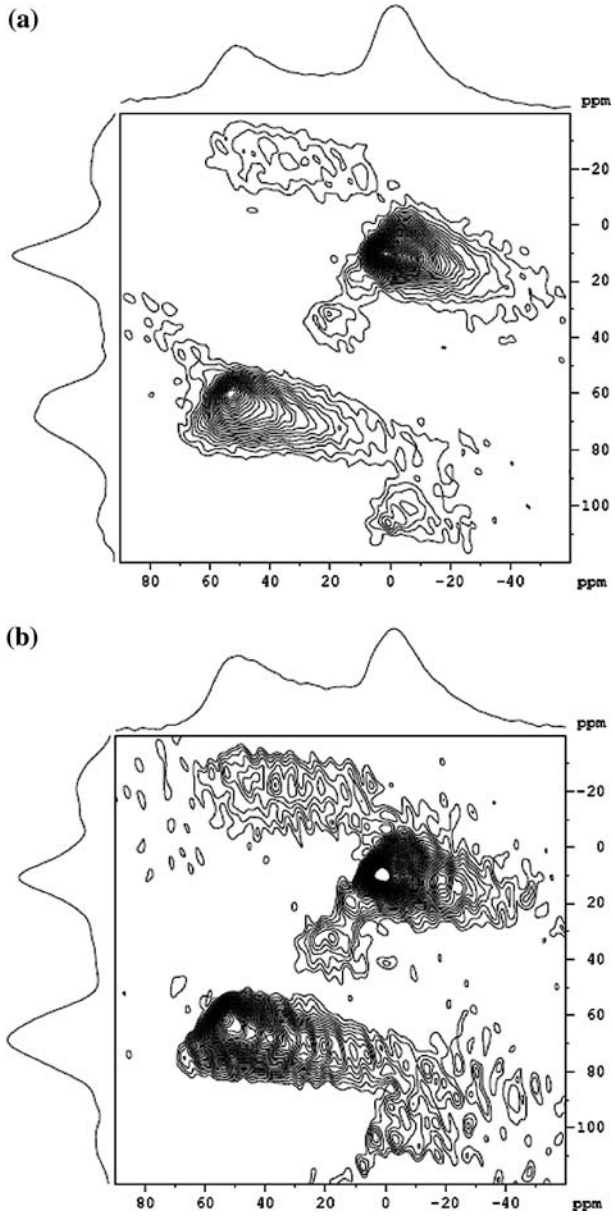

Fig. 7 ^{7}Al MQMAS spectra obtained at 104.31 MHz with a 14.0 kHz spinning rate from the F2LC cements either self-cured (**a**) or self- & photo-cured (**b**)

concentration of 6-coordinated species by 28%. This new 6-coordinated aluminium is the portion of aluminium that is leached from the glass particles to the cement matrix and partially responsible for the cross-linking of the polymer chains. In the case of the photo-cured cement, 4- and 5-coordinated species reduce their concentrations by 14% and 6%, respectively, and 6-coordinated species increases by 20%. Because similar amounts of 4-coordinated Al are leached out during SC and SPC reactions, it may be concluded that less 6-coordinated aluminium concentration in SPC cement is only due to a lower extent of 5-coordinated Al leaching. Additionally, the aluminium leaching of SC cement is 8% higher than SPC cement's. Hence, the photoirradiation and the corresponding polymer formation inhibit the evolution of the acid–base reactions more extensively then self-curing. Compared to the results obtained for the conventional GIC [10] (46% of the aluminium leached) the leaching percentages are much lower for the RMGIC, either self-cured or self- & photo-cured.

In glasses, silicon usually adopts a tetrahedral configuration with the silicon atom in the centre of the tetrahedra and oxygens in the corners; however, ^{29}Si NMR glass signals are broad due to the presence of distributions of interatomic distances and angles. ^{29}Si MAS NMR spectra of the solid component, SC and SPC cements were obtained (not shown here). The glass signal was observed at –95.4 ppm with FWHM of about 18 ppm, and is assigned to Q^4 units with 1 or 2 Al in the second coordination sphere. Only slight upfield (lower δ) shifts were observed in the frequency of ^{29}Si resonance either in SC or in SPC cement spectra: 1.4 ppm and 1.7 ppm, respectively (FWHM of about 20 ppm). This observation is consistent with a decrease in the number of aluminium species present in the silicon second coordination sphere; nevertheless, further conclusions cannot be inferred due to the small spectral effects.

3.4 Surface characterization

SEM micrographs of SC and SPC cements are presented in Fig. 8a and b, respectively. The existence of voids and cracks are observed in the micrographs of both samples, which are due to sample polishing and

Table 3 Concentration and NMR parameters for the ^{27}Al species in the glass and in SC and SPC F2LC cements, obtained by fitting the experimental 1D spectra using the software program *dmfit* [35]

Al coordination	Glass			SC cement			SPC cement		
	δ_{iso} (ppm)	C_q (MHz)	Concentration (mol%)	δ_{iso} (ppm)	C_q (MHz)	Concentration (mol%)	δ_{iso} (ppm)	C_q (MHz)	Concentration (mol%)
4	58.5	5.0	65	59.4	4.9	50	58.7	4.7	51
5	25.4	4.8	27	25.4	4.3	14	25.3	4.6	21
6	1.4	4.0	8	4.7	3.9	36	4.7	4.0	28

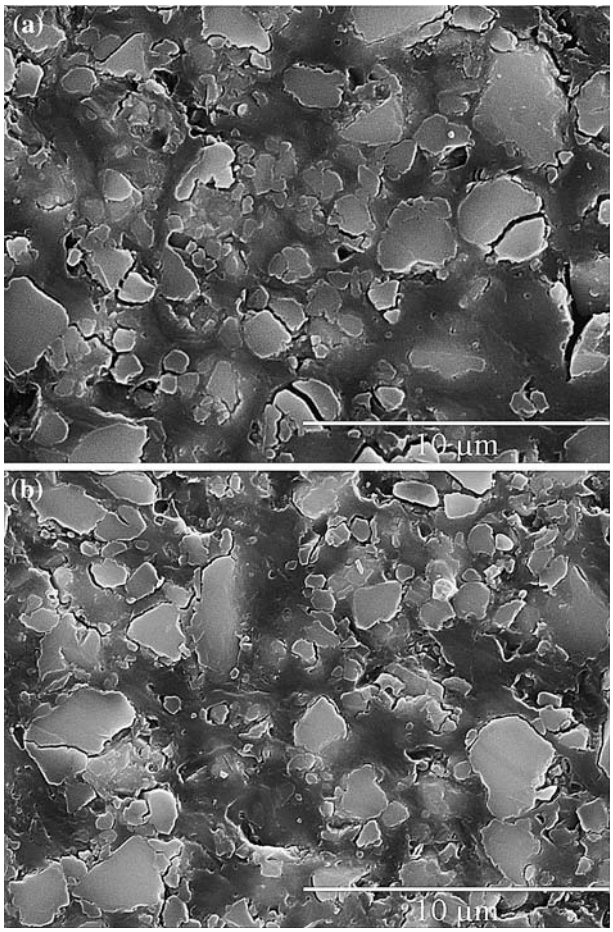

Fig. 8 SEM micrographs, with a magnification of 5,000×, obtained from: (**a**) F2LC self-cured cement, (**b**) F2LC self- & photo-cured cement

vacuum condition. Additionally, there is clear evidence for a higher concentration of glass particles in the photo-cured cement, which is consistent with shrinkage, reported on the polymerization of methacrylate monomers [25]. This problem, which is present not only in the plane of the micrograph but also in a plane perpendicular to this one, induces roughness to the sample because only the cement matrix shrinks, not the glass particles.

4 Conclusions

Curing reactions, ^{1}H, ^{13}C, ^{27}Al and ^{29}Si nuclei environments and surface of the commercial available F2LC RMGIC could be characterized using a variety of NMR imaging and spectroscopic techniques and SEM analysis.

Overall, the time constants obtained for SC cement agree well with the previously reported data on a conventional GIC [10] but, while gel forms at a similar rate in both materials, an average time constant 15 h longer was obtained for the maturation process in this RMGIC. The kinetics of the acid–base reactions seems to be similar to conventional GICs, and, for the photopolymerization reactions, two processes could be distinguished, which were tentatively assigned to chemically and diffusion controlled reactions. The time constant obtained for the chemically controlled process is of the same order of magnitude of values reported on other studies of resins [18, 31], being consistent with photoirradiation curing phenomena.

Aluminium leached from the glass particles was quantified. While in the case of SC cement 28% of the aluminium was leached to the cement matrix, only 20% was leached in the case of the photo-cured cement; this observation is consistent with an inhibition of the acid–base reaction when photopolymerization is promoted. It was shown also that less 6-coordinated aluminium concentration in SPC cement is only due to a lower extent of 5-coordinated Al leaching.

These results indicate that SPC cements with higher cross-link densities, hence improved performance, should be attained if longer time intervals between paste preparation and light-irradiation onset would be used, in order to enable increasing the concentration of leached cations that may act as cross-linkers. Moreover, SEM micrographs show that photopolymerization induces 3-dimensional shrinkage of the cement matrix.

Acknowledgments RP gratefully acknowledge the Ph.D. research grant (BD/21572/99) from the Portuguese Foundation for Science and Technology. Part of this work was performed on the frame of the research project POCTI/33193/FCB/2000 (FCT/FEDER). GC Europe is acknowledged for kindly supplying Fuji II LC.

References

1. B. E. KENT, B. G. LEWIS and A. D. WILSON, *Br. Dent. J.* **135** (1973) 322
2. A. D. WILSON and J. W. NICHOLSON, in "Acid-base cements: Their biomedical and industrial applications" (Cambridge University Press, Cambridge, 1993)
3. A. D. WILSON and J. W. MCLEAN in "Glass-Ionomer Cement" (Quintessence Books, Chicago, 1988)
4. A. D. WILSON, *Chem. Soc. Rev.* **7** (1978) 265
5. K. A. MILNE, N. J. CALOS, J. H. ODONNELL, C. H. L. KENNARD, S. VEGA and D. MARKS, *J. Mater. Sci. Mater. Med.* **8** (1997) 349
6. B. E. KENT, B. G. LEWIS and A. D. WILSON, *J. Dent. Res.* **58** (1979) 1607
7. S. CRISP, M. A. PRINGUER, D. WARDLEWO and A. D. WILSON, *J. Dent. Res.* **53** (1974) 1414
8. J. W. NICHOLSON, P. J. BROOKMAN, O. M. LACY and A. D. WILSON, *J. Dent. Res.* **67** (1988) 1451

9. S. MATSUYA, T. MAEDA and M. OHTA, *J. Dent. Res.* **75** (1996) 1920
10. R. PIRES, T.G. NUNES, I. ABRAHAMS, G. E. HAWKES, C. M. MORAIS and C. FERNANDEZ, *J. Mater. Sci. Mater. Med.* **15** (2004) 201
11. W. D. COOK, *J. Biomed. Mater. Res.* **17** (1983) 1015
12. J. W. NICHOLSON, *Biomaterials* **19** (1998) 485
13. B. M. CULBERTSON, *Prog. Polym. Sci.* **26** (2001) 577
14. R. S. MATHIS and J. L. FERRACANE, *Dent. Mater.* **5** (1989) 355
15. S. B. MITRA, *J. Dent. Res.* **70** (1991) 72
16. A. U. J. YAP, *J. Mater. Sci. Mater. Med.* **8** (1997) 413
17. H. M. ANSTICE and J. W. NICHOLSON, *J. Mater. Sci. Mater. Med.* **5** (1994) 299
18. T. G. NUNES, G. GUILLOT, S. G. PEREIRA and R. PIRES, *J. Phys. D Appl. Phys.* **35** (2002) 1251
19. P. J. MCDONALD, *Prog. Nucl. Magn. Reson. Spectrosc.* **30** (1997) 69
20. N. MALICKI, L. MAFRA, A.-A. QUOINEAUD, J. ROCHA, F. THIBAULT-STARZYK and C. FERNANDEZ, *Solid State Nucl. Magn. Reson.* **28** (2005) 13
21. G. ENGELHARDT and H. KOLLER, in ''Solid State NMR II: Inorganic Matter'', Edited by: P. DIEHL, E. FLUCK, H. GÜNTHER, R. KOSFELD and J. SEELIG (Springer-Verlag, Berlin, 1994)
22. A. A. SAMOILENKO, D. Y. ARTEMOV and L. A. SIBELDINA, *JETP Lett.* **47** (1988) 417
23. T. NUNES, E. W. RANDALL, A. A. SAMOILENKO, P. BODART and G. FEIO, *J. Phys. D Appl. Phys.* **29** (1996) 805
24. C. H. LLOYD, S. N. SCRIMGEOUR, G. HUNTER, J. A. CHUDEK, D. M. LANE and P. J. MCDONALD, *J. Mater. Sci. Mater. Med.* **10** (1999) 369
25. S. G. PEREIRA, T. G. NUNES and S. KALACHANDRA, *Biomaterials* **23** (2002) 3799
26. T. G. NUNES, R. PIRES, J. PERDIGÃO, A. AMORIM and M. POLIDO, *Polymer* **42** (2001) 8051
27. C. H. LLOYD, S. N. SCRIMGEOUR, D. M. LANE, G. HUNTER and P. J. MCDONALD, *Dent. Mater.* **17** (2001) 381
28. S. CHATTERJI, *Cem. Concr. Res.* **18** (1988) 615
29. S. G. PEREIRA, N. REIS and T. G. NUNES, *Polymer* **46** (2005) 8034
30. L. C. MENDES, A. D. TEDESCO and M. S. MIRANDA, *Polym. Test.* **24**(2005) 418
31. G. GUILLOT, T. G. NUNES, J. P. RUAUD and M. POLIDO, *Polymer* **45** (2004) 5525
32. J. H. BALTISBERGER, Z. XU, J. F. STEBBINS, S. H. WANG and A. PINES, *J. Am. Chem. Soc.* **118** (1996) 7209
33. J. F. STEBBINS, S. KROEKER, S. K. LEE and T. J. KICZENSKI, *J. Non Cryst. Solids* **275** (2000) 1
34. J. P. AMOUREUX, C. FERNANDEZ and L. FRYDMAN, *Chem. Phys. Lett.* **259** (1996) 347
35. L. FRYDMAN and J. S. HARWOOD, *J. Am. Chem. Soc.* **117** (1995) 5367
36. D. MASSIOT, F. FAYON, M. CAPRON, I. KING, S. LE CALVE, B. ALONSO, J. O. DURAND, B. BUJOLI, Z. H. GAN and G. HOATSON, *Magn. Reson. Chem.* **40** (2002) 70